An Analysis of Gipps' Car-Following Model of Highway Traffic *

R. Eddie Wilson†

Abstract

A mathematical analysis of P.G. Gipps' (1981) car-following model is performed. This model is of practical importance as it powers the UK Transport Research Laboratory highway simulation package SISTM. Uniform flow solutions and a speed-headway function are derived under simplifying conditions. A linear stability analysis of uniform flow is then performed, and stable and unstable regimes are identified. Finally, some numerical simulations for a variety of parameter regimes are presented.

1 Introduction

The car-following methodology for the simulation and analysis of highway traffic, which models vehicles as discrete entities moving in continuous space, originates with Chandler (1958) [3] and Gazis (1961) [5], but has recently been the subject of much attention in the applied mathematics and theoretical physics literature.

This interest has been sparked by the model of Bando *et al* (1995) [2], which possesses the following property: in certain conditions, a uniform flow of traffic (in which all vehicles move at the same speed, maintaining constant spacing) can lose stability. This means that small fluctuations to the flow will grow rapidly, and it has been conjectured that the Bando model thus captures the essence of the mechanism for flow breakdown and spontaneous traffic jam formation.

Holland (1998) [7] has subsequently identified the same loss of stability effect in a number of other car-following models. However, one model outside Holland's framework is that introduced by Gipps (1981) [6]. This model is the basis of the UK Transport Research Laboratory's traffic simulation package SISTM [10], and the network simulation software PARAMICS [4], and thus has great practical importance.

Gipps' model contains a number of parameters which purport to model different behavioural features of drivers, and is thus rather more complicated than the reductionist models which one usually finds in the mathematical literature. This degree of realism is desirable for simulation software involved in the normative testing of particular highway scenarios. However, in such simulations, it can be unclear how traffic flows relate to particular parameters, without repeating the (computationally expensive) simulation at many points in parameter space. Thus in our view, there is scope for the mathematical analysis of simplified scenarios: at the very least, one might identify parameter regimes which merit further investigation with one's simulation software.

The aim of this paper is to apply such a mathematical analysis to Gipps' model. The two principal simplifying assumptions which will hold for the duration of our analysis are that 1. we consider a single lane highway only; multi-lane scenarios with lane changing effects are not considered; and 2. we assume that the characteristics of all vehicles and drivers are the same. This latter assumption simplifies calculations but is probably not necessary for our analysis to work. When vehicles/drivers differ, it is likely that techniques similar to those used on the Bando model by Mason and Woods (1997) [8], will extend the scope of our analysis. Here (in Section 6) we perform some simulations of this inhomogeneous situation: results are similar to those when all vehicles/drivers are equal, and this justifies our simplified approach.

Our scheme is as follows: in Section 2, we review the details of Gipps' model, giving a brief description of the parameters. Strictly speaking, this model gives a large system of differential difference equations. However, Gipps' idea was to integrate these equations using a coarse time step equal to the reaction time of

*Submitted IMA Journal on Applied Mathematics 10th October 2000, accepted 12 March 2001.

†Department of Engineering Mathematics, University of Bristol, Bristol BS8 1TR, United Kingdom
Email: RE.Wilson@bristol.ac.uk

drivers. This is a crude approach: however, we follow it faithfully, and thus derive a large system of coupled maps for the discrete time evolution of vehicles' displacements and velocities. The remainder of the paper is concerned with the analysis and simulation of the system of maps, rather than the original differential difference equation problem.

In Section 3, we analyse the uniform flow solutions of Gipps' model. In uniform flow, all vehicles travel at the same time independent speed and thus their spacings are time independent. Further if driving characteristics are the same for all vehicles, the separation h of consecutive vehicles (known as the headway) will be the same throughout the flow. For safety reasons, vehicles must travel slower if they are closer together (the classic example being the so-called *two second rule* of the UK Highway Code [9]). We show that there is usually a unique uniform flow for any headway $h > 0$; denoting the speed of uniform flow by V, we thus find a monotone increasing *speed-headway function* $V(h)$. We also find an unphysical parameter regime where the speed-headway function is not well defined.

In Section 4, we consider the evolution of small perturbations imposed on the uniform flow solutions of Section 3. In particular, we would like to know whether perturbations decay in time (corresponding to a stable uniform flow) or whether they grow, giving rise to flow breakdown. We conclude with a complex quadratic characteristic equation for an eigenvalue λ, whose modulus must be less than one for stability.

Section 5 continues with an analysis of the quadratic characteristic equation derived in Section 4. This equation is parameterised by an angle $\xi \in [0, 2\pi)$, which determines the spatial wavelength of the perturbations under consideration. To prove stability of a uniform flow, one must show $|\lambda| < 1$ for all choices of $\xi \in [0, 2\pi)$. To show instability one need only find a single ξ for which $|\lambda| > 1$.

We give an explicit analysis which shows that the $\xi = 0$ (space independent) mode can only be unstable in the parameter regime where the speed-headway function is not well defined.

We then present graphs which indicate that if any mode is unstable, then the $\xi = \pi$ mode (which has shortest wavelength) is also unstable. We therefore perform an explicit analysis of the $\xi = \pi$ case. We thus identify stable uniform flows and a physical parameter regime where uniform flow is unstable. We show analytically that uniform flow is destabilised by reducing the parameters which correspond to 1. drivers' estimates of the braking of the vehicle ahead, and 2. drivers' *safety margin* (a quantity with units time); or 3. by vehicles driving faster. Gipps identified the first mechanism in a primitive numerical simulation: we now have a complete analytical identification of stable and unstable regimes.

In Section 6, we present some simulations which illustrate the different stability features of Gipps' model. In particular, in the unstable regime, we show the formation of travelling waves, which resemble the shocks one experiences when driving down the motorway. We also indicate that in some parameter regimes, there are problems with the existence of a physical solution for all positive times.

Further, we show that similar solutions are observed if vehicles are allowed to have different characteristics from each other, justifying the "all vehicles equal" assumption we make during our analysis.

Finally, in Section 7, we mention some possibilities for further work.

2 Review of Gipps' model

In this section, we provide the mathematical details of Gipps' car-following model: see [6] for the derivation. The model takes the form of a system of differential difference equations involving the common reaction time τ of drivers. Gipps implements this system by setting the time step in his integration package equal to τ, and here we formulate the (discrete time) system of maps arising from this approach when the Trapezoidal rule integration scheme is used.

Figure 1 shows the basic situation. We consider a total of N vehicles labelled $1, 2, \ldots, n-1, n, n+1, \ldots, N$ on a single lane road. Car number 1 is the lead car, and cars move in an increasing x direction, with displacements x_1, x_2, ..., and with positive velocities v_1, v_2, ... The *headway* of vehicle n is given by $h_n := x_{n-1} - x_n$, and the length of each vehicle is S_{n-1} (although we may include a safety distance in this value into which it is undesirable to encroach, so that $h_n < S_{n-1}$ corresponds to an incident which may involve vehicles crashing).

Gipps' modelling leads to a formula

$$v_n(t+\tau) = \min\left[v_n(t) + 2.5A_n\tau\left(1-\frac{v_n(t)}{V_n^{\max}}\right)\left(0.025+\frac{v_n(t)}{V_n^{\max}}\right)^{1/2}, \right.$$
$$\left. -B_n\left(\frac{\tau}{2}+\theta\right) + \sqrt{\left[B_n^2\left(\frac{\tau}{2}+\theta\right)^2 + B_n\left\{2\left\{x_{n-1}(t)-x_n(t)-S_{n-1}\right\} - \tau v_n(t) + \frac{v_{n-1}(t)^2}{\hat{B}_{n-1}}\right\}\right]}\right], \quad (2.1)$$

giving the speed of each vehicle at time $t+\tau$ in terms of its speed at the earlier time t. If the road is uncongested and the headway of vehicle n is large, then the first argument of the min is attained, and vehicle n accelerates freely according to a law fitted from empirical traffic data. (SI units are used throughout.) Here $A_n > 0$ is an acceleration parameter, and $V_n^{\max}$ is the maximum speed at which driver n wishes to travel. The parameter τ corresponds to a reaction time, which Gipps assumes is equal for all drivers.

However, we are interested in congested situations where headways are smaller, and the second argument of the min of (2.1) is attained. In this regime the speed of each vehicle is limited by the behaviour of the vehicle in front. The fundamental assumption is that each driver sets his/her speed so as to be able to come to a stop without hitting the vehicle in front, supposing that the vehicle in front decelerates at no more than a certain rate.

To be more precise, driver n estimates that vehicle $n-1$ will not wish to brake harder than rate $\hat{B}_{n-1} > 0$, and controls his/her speed so that if this level of braking does occur, then by braking at rate B_n, he/she will be able to come to a stop without encroaching in the safety distance. Factored into this derivation is that driver n cannot commence braking until a reaction time τ has elapsed. However, it is supposed that drivers also allow a *safety margin* time θ. This models the conservative behaviour of drivers who select speeds so that if they commence braking at time θ after their reaction time has elapsed, they are still able to come to a stop safely.

(Note we have made some notational changes from [6]: in particular positive quantities represent both braking and acceleration rates, and we use capital or Greek letters to distinguish parameters which are provided from lower case variables which are solved for. We have also retained the safety margin parameter θ: Gipps sets it equal to $\theta = \tau/2$ at an early stage of his derivation.)

Assuming that all vehicles have the same parameters and all drivers the same characteristics, we may drop the subscripts from parameters, and note that the second regime of (2.1) can be written

$$v_n(t+\tau) = F(x_{n-1}(t) - x_n(t),\, v_n(t),\, v_{n-1}(t)), \quad (2.2)$$

where

$$F(\phi,\psi,\chi) := -B\left(\frac{\tau}{2}+\theta\right) + \sqrt{\left[B^2\left(\frac{\tau}{2}+\theta\right)^2 + B\left\{2(\phi-S) - \tau\psi + \frac{\chi^2}{\hat{B}}\right\}\right]}. \quad (2.3)$$

The four parameters B, $\hat{B}$, τ, and θ will be the key ones in our linear stability analysis. In particular, the relative sizes of actual braking B and perceived breaking $\hat{B}$ are crucial.

At this point, it is instructive to note the partial derivatives of F,

$$\frac{\partial}{\partial\phi}F(\phi,\psi,\chi) = BQ, \quad \frac{\partial}{\partial\psi}F(\phi,\psi,\chi) = -\frac{1}{2}B\tau Q, \quad \text{and} \quad \frac{\partial}{\partial\chi}F(\phi,\psi,\chi) = \frac{B}{\hat{B}}\chi Q, \quad (2.4)$$

where

$$Q = \left[B^2\left(\frac{\tau}{2}+\theta\right)^2 + B\left\{2(\phi-S) - \tau\psi + \frac{\chi^2}{\hat{B}}\right\}\right]^{-1/2}, \quad (2.5)$$
$$= \frac{1}{F(\phi,\psi,\chi) + B\left(\frac{\tau}{2}+\theta\right)}, \qquad > 0. \quad (2.6)$$

Therefore $\partial F/\partial\phi > 0$, $\partial F/\partial\psi < 0$, $\partial F/\partial\chi > 0$. Thus we might talk of *Gipps-like* models to be those of the form of (2.2), where the speed of a vehicle at time $t+\tau$ is inhibited by its own speed at time t, but enhanced

by the speed of the vehicle ahead, and enhanced by the headway. We use the term *standard Gipps model* when the nonlinearity is prescribed by (2.3).

Now let us address how (2.2) can be used to formulate a closed mathematical system which predicts the positions x_n and velocities v_n of all N vehicles for all positive time. The most natural procedure is to supplement (2.2) with

$$\frac{\mathrm{d}}{\mathrm{d}t}x_n(t) = v_n(t), \tag{2.7}$$

to obtain a system of $N + N$ differential difference equations (rather like a system of differential delay equations). If initial data for positions and velocities are prescribed for $t \in [-\tau, 0]$, and a suitable boundary condition is prescribed to fix the motion of the lead car for $t > 0$, then (2.2,2.7) should predict displacements and velocities of all vehicles for all time. However a boundary condition for the lead car is not required if the vehicles are placed on a circular road, because vehicle 1 would have its speed determined by vehicle N. This is our approach from Section 4 onwards.

Note that global existence of physical solutions for $t > 0$ is not guaranteed: e.g., we have not proved that the square root in (2.1) always gives rise to a real speed. Indeed, in Section 6 we present simulations which show how solutions may become complex for inappropriate parameter choices.

The analysis of a differential difference equation system like (2.2,2.7) is technically difficult. However, Gipps observed numerically that this system behaves well when integrated with time step τ. (Indeed, reducing computational cost in this crude manner was the motivation for his model.) Thus we analyse the system obtained by replacing (2.7) with its discretisation by a suitable integration scheme, such as the Trapezoidal rule

$$\frac{x_n(t+\tau) - x_n(t)}{\tau} = \frac{1}{2}v_n(t) + \frac{1}{2}v_n(t+\tau), \tag{2.8}$$

which rearranged yields

$$x_n(t+\tau) = x_n(t) + \frac{\tau}{2}v_n(t) + \frac{\tau}{2}v_n(t+\tau). \tag{2.9}$$

It is not at all clear how the dynamics of the discretisation are affected by the integration rule used. We do not analyse this question here, but conjecture that the dynamics should be similar for all A-stable integration schemes. Henceforth, we consider only the system arising from the Trapezoidal rule.

Note that formula (2.9) is not implicit, because an explicit formula for $x_n(t+\tau)$ in terms of values at the earlier time step may be derived, since formula (2.2) for $v_n(t+\tau)$ is explicit. Thus we obtain

$$x_n(t+\tau) = x_n(t) + \frac{\tau}{2}v_n(t) + \frac{\tau}{2}F(x_{n-1}(t) - x_n(t),\, v_n(t),\, v_{n-1}(t)). \tag{2.10}$$

The key is to note that values of displacement and velocity at time $t+\tau$ now depend only on values at time t, and not on values at intermediate times. Therefore, we may dispense with continuous time, and define $t_m := t_0 + m\tau$, and let $x_{m,n} := x_n(t_m)$, $v_{m,n} := v_n(t_m)$, to obtain the system of $2N$ maps

$$\begin{aligned} x_{m+1,n} &= x_{m,n} + \frac{\tau}{2}v_{m,n} + F(x_{m,n-1} - x_{m,n},\, v_{m,n},\, v_{m,n-1}), \\ v_{m+1,n} &= F(x_{m,n-1} - x_{m,n},\, v_{m,n},\, v_{m,n-1}). \end{aligned} \tag{2.11}$$

for the discrete time evolution of all displacements and velocities.

3 Uniform flow and the speed-headway function

In this section, we analyse the uniform flow solutions of the system of maps (2.11). In uniform flow, all vehicles travel at the same speed (v^* say), so that their spacings are time independent. Let us also suppose that all vehicles have the same properties, and the same common headway (h^* say). Here we find the *speed-headway* function V which gives $v^* = V(h^*)$. We expect V to be an increasing function, because (for safety reasons) vehicles will drive more slowly as their spacing decreases.

Our uniform flow solution takes the form

$$\begin{aligned} v_{m,n} &= v^*, \qquad \forall m, n \\ x_{m,n} &= x_0 + mv\tau^* - nh^*. \end{aligned} \tag{3.1}$$

However, it is more convenient to change variables so that uniform flow is a steady state solution. This may be achieved by re-casting system (2.11), which describes the joint evolution of displacements and velocities, as a system which describes the joint evolution of headways and velocities. Noting that

$$h_{m+1,n} = x_{m+1,n-1} - x_{m+1,n}, \tag{3.2}$$

from (2.11) we may derive

$$\begin{aligned} h_{m+1,n} &= h_{m,n} + \frac{\tau}{2}(v_{m,n-1} - v_{m,n}) + \frac{\tau}{2}\left\{F(h_{m,n-1},\, v_{m,n-1},\, v_{m,n-2}) - F(h_{m,n},\, v_{m,n},\, v_{m,n-1})\right\}, \\ v_{m+1,n} &= F(h_{m,n},\, v_{m,n},\, v_{m,n-1}). \end{aligned} \tag{3.3}$$

Uniform flow solutions are now steady state solutions in the form

$$h_{m,n} = b^*, \quad v_{m,n} = v^*, \qquad \forall m, n. \tag{3.4}$$

It follows from (3.3) that such h^*, v^* satisfy

$$v^* = F(h^*, v^*, v^*). \tag{3.5}$$

The desire is now to consider this formula and isolate v^* as a function of h^*, and thus give the speed-headway function. Consider the definition (2.3) of F: we isolate the square root and square to give

$$\left[v^* + B\left(\frac{\tau}{2} + \theta\right)\right]^2 = \left[B^2\left(\frac{\tau}{2} + \theta\right)^2 + B\left\{2(h^* - S) - \tau\psi + \frac{v^{*2}}{\hat{B}}\right\}\right], \tag{3.6}$$

which may be expanded and re-written as a quadratic in v^*,

$$\left(\frac{B}{\hat{B}} - 1\right)v^{*2} - 2B(\tau + \theta)v^* + 2B(h^* - S) = 0. \tag{3.7}$$

In the special case $B = \hat{B}$, this is a linear equation for v^* whose solution is trivial. However, the predicted v^* is only valid if $0 < v^* < V^{\max}$. To see this, first note that $v^* < 0$ corresponds to an unphysical flow where vehicles reverse. Secondly, note that if $v^* > V^{\max}$, then the derivation of (3.5) is invalid. This is because the first argument of the min of (2.1) is negative (hence less than v^*) and is thus attained. To expand upon this idea, note that if all velocities are steady and equal to v^*, then (2.1) yields

$$v^* = \min\left[v^* + A\tau\left(1 - \frac{v^*}{V^{\max}}\right)\left(0.025 + \frac{v^*}{V^{\max}}\right)^{1/2},\, F(h^*, v^*, v^*)\right]. \tag{3.8}$$

Hence uniform flow with $v^* = V^{\max}$ is a solution provided h^* is sufficiently large for $F(h^*, V^{\max}, V^{\max}) > V^{\max}$ to hold, so that the first argument of the minimum is attained.

Thus for $\hat{B} = B$, we arrive at the speed-headway function

$$V(h) = \mathrm{mid}\left[0,\, \frac{h - S}{\tau + \theta},\, V^{\max}\right], \tag{3.9}$$

where

$$\mathrm{mid}(0, v, V^{\max}) := \min\left\{V^{\max}, \max(0, v)\right\}, \tag{3.10}$$

defines the mid function. See Figure 2. Note in particular, for Gipps' recommended parameter values $\tau = 2/3$s and $\theta = \tau/2$, the linear regime of (3.9) corresponds to a one second car-following law.

For $B \neq \hat{B}$, (3.7) may be solved to give

$$v^* = \frac{B(\tau+\theta)}{\left(\frac{B}{\hat{B}}-1\right)}\left[1 \pm \sqrt{\left\{1 - \frac{2(h^*-S)\left(\frac{B}{\hat{B}}-1\right)}{B(\tau+\theta)^2}\right\}}\right], \tag{3.11}$$

using the standard formula for the solution of a quadratic equation. The solution possibilities are now governed by whether $\hat{B} > B$, or vice versa.

For $\hat{B} > B$, the magnitude of the square root is larger than one, so one obtains roots of opposite signs: as before, only the positive root is physical. Similar considerations to the $\hat{B} = B$ case give the speed-headway function

$$V(h) = \text{mid}\left[0,\ \left(\frac{\tau+\theta}{\frac{1}{B}-\frac{1}{\hat{B}}}\right)\left[-1 + \sqrt{\left\{1 + \frac{2(h-S)\left(\frac{1}{B}-\frac{1}{\hat{B}}\right)}{(\tau+\theta)^2}\right\}}\right],\ V^{\max}\right]. \tag{3.12}$$

See Figure 3.

However, when $\hat{B} < B$, (i.e., when the estimated rate of braking is less than the actual rate), both solutions are positive for $h^* > S$. See Figure 4. It seems natural to take the lower (i.e. slower) branch of the resulting parabolic curve. It may be shown that the rightmost point of the parabola occurs at $V = (\tau+\theta)/(1/\hat{B} - 1/B)$. Hence problems occur if

$$V^{\max} > \frac{\tau+\theta}{\frac{1}{\hat{B}}-\frac{1}{B}}, \tag{3.13}$$

because there is no continuous way of joining the two solution parts $v^* = F(h^*, v^*, v^*) < V^{\max}$, and $v^* = V^{\max} < F(h^*, V^{\max}, V^{\max})$, without $V(h)$ being multi-valued at some points. However, it is widely accepted in the traffic engineering community that the speed-headway function should be a single-valued non-decreasing function, so we consider this situation to be unphysical.

However when (3.13) fails, we may write down the speed-headway function

$$V(h) = \text{mid}\left[0,\ \left(\frac{\tau+\theta}{\frac{1}{\hat{B}}-\frac{1}{B}}\right)\left[1 - \sqrt{\left\{1 - \frac{2(h-S)\left(\frac{1}{\hat{B}}-\frac{1}{B}\right)}{(\tau+\theta)^2}\right\}}\right],\ V^{\max}\right]. \tag{3.14}$$

We remark that the speed-headway functions (3.9), (3.12), and (3.14) for uniform flow depend only upon the sum $\tau+\theta$, and not on the reaction time τ and safety margin θ parameters separately. However, we shall see in Section 5 that dynamic behaviour may depend on τ and θ independently of each other. Note also that the speed headway function involves $(1/\hat{B} - 1/B)$, and not the braking rates $\hat{B}$ and B independently of each other.

4 Linear stability of uniform flow: formulation

We now consider the evolution of small perturbations superimposed on the uniform flow solutions of Section 3. We want to know whether perturbations decay (in which case we say that the uniform flow is stable), or whether they grow (in which case flow breakdown may ensue). This section considers only the mathematical formulation of the stability problem, which is solved later in Section 5.

To begin, we substitute

$$\begin{aligned} h_{m,n} &= h^* + \tilde{h}_{m,n}, \\ v_{m,n} &= v^* + \tilde{v}_{m,n}, \end{aligned} \tag{4.1}$$

in system (3.3). Here $v^* = V(h^*)$ (V is the speed headway function) and $\tilde{h}_{m,n}$ and $\tilde{v}_{m,n}$ are small perturbations to the headways and velocities of the uniform flow under consideration. We then perform the usual

Taylor series expansions: leading order terms cancel out, and if we neglect quadratic and higher order terms, we obtain

$$\tilde{h}_{m+1,n} = \tilde{h}_{m,n} + \frac{\tau}{2}(\tilde{v}_{m,n-1} - \tilde{v}_{m,n}) + \frac{\tau}{2}\left\{(\partial_1 F)(\tilde{h}_{m,n-1} - \tilde{h}_{m,n}) + (\partial_2 F)(\tilde{v}_{m,n-1} - \tilde{v}_{m,n}) + (\partial_3 F)(\tilde{v}_{m,n-2} - \tilde{v}_{m,n-1})\right\},$$

and

$$\tilde{v}_{m+1,n} = (\partial_1 F)\tilde{h}_{m,n} + (\partial_2 F)\tilde{v}_{m,n} + (\partial_3 F)\tilde{v}_{m,n-1}, \tag{4.2}$$

as a system of $2N$ linear maps for the evolution of (small) headway and velocity perturbations. Here

$$(\partial_1 F) := \frac{\partial}{\partial\phi}F(\phi,\psi,\chi)_{|(h^*,v^*,v^*)}, \qquad (\partial_2 F) := \frac{\partial}{\partial\psi}F(\phi,\psi,\chi)_{|(h^*,v^*,v^*)},$$
$$\text{and} \qquad (\partial_3 F) := \frac{\partial}{\partial\chi}F(\phi,\psi,\chi)_{|(h^*,v^*,v^*)}, \tag{4.3}$$

denote the partial derivatives of F evaluated at the uniform flow solution under consideration. For the standard Gipps model, equations (2.4) and (2.6) with the uniform flow condition (3.5) give

$$(\partial_1 F) = \frac{1}{\frac{v^*}{B} + \frac{\tau}{2} + \theta}, \qquad (\partial_2 F) = -\frac{1}{2}\frac{\tau}{\frac{v^*}{B} + \frac{\tau}{2} + \theta}, \qquad \text{and} \qquad (\partial_3 F) = \frac{\frac{v^*}{B}}{\frac{v^*}{B} + \frac{\tau}{2} + \theta}. \tag{4.4}$$

To simplify matters, we now suppose that the N vehicles are arranged on a circular road, so that vehicle 1 follows vehicle N. This implies that $h_{m,n}$ and $v_{m,n}$ (and thus $\tilde{h}_{m,n}$ and $\tilde{v}_{m,n}$) are N-periodic in the vehicle index n, because if we count N vehicles along the circular road, we return to our starting point. The periodicity in n allows expansion of $\tilde{h}$ and $\tilde{v}$ in discrete Fourier modes of wave number $k = 0, 1, 2, \ldots, N-1$. To clarify, we seek solutions of (4.2) in the form

$$\tilde{h}_{m,n} = \mathrm{Re}\left(c_h \lambda^m w^n\right), \qquad \tilde{v}_{m,n} = \mathrm{Re}\left(c_v \lambda^m w^n\right), \tag{4.5}$$

where c_h, c_v are complex constants, and w is defined by

$$w := \mathrm{e}^{i\xi}, \qquad \text{where} \qquad \xi := \frac{2k\pi}{N}. \tag{4.6}$$

This ansatz is the crux of our stability analysis, and was introduced by Bando *et al* (1995) [2] to analyse the stability of a different car-following model from that considered here.

When $\xi = 0$ (from $k = 0$), the trial mode is space independent (i.e. the same for all vehicles at a particular time). At the other extreme, $\xi = \pi$ (from $k = N/2$) corresponds to the shortest wavelength mode, where the perturbation repeats every second vehicle. Note that λ is a (possibly complex) eigenvalue whose modulus determines whether modes grow or decay in time.

On the substitution of (4.5) in (4.2), the usual simplifications give

$$\begin{aligned} \lambda c_h &= c_h + \frac{\tau}{2}c_v + \frac{\tau}{2}(w^{-1} - 1)\left\{(\partial_1 F)c_h + (\partial_2 F)c_v + (\partial_3 F)w^{-1}c_v\right\}, \\ \lambda c_v &= \left\{(\partial_1 F)c_h + (\partial_2 F)c_v + (\partial_3 F)w^{-1}c_v\right\}. \end{aligned} \tag{4.7}$$

The first equation may be simplified using the second, and rearrangement gives the system

$$\begin{aligned} (\lambda - 1)c_h &= \frac{\tau}{2}(w^{-1} - 1)(\lambda + 1)c_v, \\ \left\{\lambda - (\partial_2 F) - (\partial_3 F)w^{-1}\right\}c_v &= (\partial_1 F)c_h, \end{aligned} \tag{4.8}$$

of two simultaneous equations for λ and the ratio of the constants c_h and c_v. We are most interested in finding λ, since its modulus determines the stability of perturbations: if $|\lambda| < 1$, perturbations decay, whereas if $|\lambda| > 1$, perturbations grow.

The phase constants c_h and c_v can be eliminated from (4.8) to give

$$(\partial_1 F)\frac{\tau}{2}(w^{-1}-1)(\lambda+1) = (\lambda-1)\left\{\lambda - (\partial_2 F) - (\partial_3 F)w^{-1}\right\}, \tag{4.9}$$

and rearrangement yields

$$\lambda^2 - \left\{1 + \frac{\tau}{2}(w^{-1}-1)(\partial_1 F) + (\partial_2 F) + w^{-1}(\partial_3 F)\right\}\lambda + \left\{-\frac{\tau}{2}(w^{-1}-1)(\partial_1 F) + (\partial_2 F) + w^{-1}(\partial_3 F)\right\} = 0. \tag{4.10}$$

For any given fixed parameters and wave number, this quadratic may be solved using the standard formula to give λ. Note that this procedure works for any *Gipps-like* model and does not rely on the functional form of the nonlinearity F. However, the explicit solution is sufficiently complicated so as to not be useful in its full generality.

5 Linear stability of uniform flow: solution

In this section, we analyse the quadratic characteristic problem (4.10). One difficulty with this equation is the presence of the unit magnitude complex parameter w, which gives the wave number of the perturbation under consideration. To prove that a certain uniform flow is stable, one must show that both solutions λ satisfy $|\lambda| \leq 1$ for every choice $\xi \in [0, 2\pi)$ of ξ. However, to show that a uniform flow is unstable, one must identify only one wave number, i.e. only one $\xi \in [0, 2\pi)$, where (4.10) has a solution λ with magnitude greater than one.

Our strategy is to simplify matters by first considering space independent $\xi = 0$ perturbations, in Section 5.1. By the explicit solution of (4.10), we show that uniform flow is usually stable to perturbations of this class. This is in sharp contrast to the Bando car-following model [2], in which long wavelength perturbations are the most unstable.

We do identify one parameter regime where it is possible for uniform flow solutions to be unstable to space independent perturbations; however, this requires (3.13) to be satisfied, so that uniform flow is not uniquely defined. We consider this regime to be unphysical.

In Section 5.2 we show some numerical plots of the modulus of solutions λ against ξ. These plots indicate that if $|\lambda(\xi)| > 1$ for some ξ, then $|\lambda(\pi)| > 1$. We do not offer a proof of this result, but the numerical observations motivate the analysis of the $\xi = \pi$ case (corresponding to short wavelength perturbations which repeat every other vehicle) in Section 5.3.

Fortunately, the onset of instability of the $\xi = \pi$ mode may be found explicitly, and consequently, we have an explicit sufficient condition for the instability of uniform flow. If one believes that the $\xi = \pi$ mode is the most unstable in the sense just described, then our condition is also necessary for instability, and we have a complete description of stable and unstable parameter regimes.

The reader interested only in the stability result, and not its derivation, should go straight to equation (5.13) and the discussion which follows. Here we remark simply that our analytical result is in accord with the simulations of Gipps, who found uniform flow destabilised as $\hat{B}$ is decreased. However, in addition, we now understand the role of the other parameters B, τ, θ, and v^*.

5.1 Long wavelength perturbations: $\xi = 0$

We take wave number $k = 0$, so that $\xi = 0$ and $w = 1$. Characteristic equation (4.10) thus becomes

$$\lambda^2 - \{1 + (\partial_2 F) + (\partial_3 F)\}\lambda + \{(\partial_2 F) + (\partial_3 F)\} = 0, \tag{5.1}$$

which factorises simply to yield the solutions

$$\lambda = 1 \qquad \text{and} \qquad \lambda = (\partial_2 F) + (\partial_3 F). \tag{5.2}$$

The first solution is present because we have a continuous range of uniform flow solutions of different speeds, and neutral stability within this family. For the standard Gipps model, (4.4) gives the latter solution as

$$\lambda = \frac{\frac{v^*}{\hat{B}} - \frac{\tau}{2}}{\frac{v^*}{B} + \frac{\tau}{2} + \theta}, \tag{5.3}$$

which is real. Hence for this mode to be unstable, we require either $\lambda < -1$, or $\lambda > 1$. If $\lambda < -1$, then

$$\left(\frac{1}{\hat{B}} + \frac{1}{B}\right) v^* \leq -\theta, \tag{5.4}$$

which is impossible, since the left hand side is positive and the right hand side is negative. Thus for instability of the space independent mode, we require $\lambda > 1$, which implies

$$v^* > \frac{\tau + \theta}{\frac{1}{\hat{B}} - \frac{1}{B}}. \tag{5.5}$$

In this case, note that inequality (3.13) holds, since $v^* < V^{\max}$. Hence uniform flow is not well defined for such parameter values and this seems to be an unphysical scenario.

5.2 Numerical evaluation of eigenvalues

In this section, we solve (4.10) using the explicit formula, and present numerical plots giving the modulus of λ as a function of wave number parameter ξ, for a number of different choices of physical parameters. The findings are

- Uniform flow is destabilised as the estimated breaking rate $\hat{B}$ is decreased.
- If $|\lambda(\xi)| > 1$ for some ξ, then $|\lambda(\pi)| > 1$. This motivates the explicit analysis of the $\xi = \pi$ case in Section 5.3.

Firstly, Figures 5 and 6 describe solutions λ of (4.10) for the parameter choices $B = 3.0\text{ms}^{-2}$, $\tau = 2/3\text{s}$, $\theta = 1/3\text{s}$, and uniform flow speed $v^* = 20.0\text{ms}^{-1}$. Figure 5 has estimated breaking parameter $\hat{B} = 3.5\text{ms}^{-2}$, whereas Figure 6 takes $\hat{B} = 2.5\text{ms}^{-2}$. These parameter values are taken from a pair of simulations carried out by Gipps [6]. Each plot shows the moduli of solutions λ as functions of the wave number parameter ξ. In each case we take only $\xi \in [0, \pi]$, because of even symmetry. To each plot we add a horizontal line of height one, so that stable and unstable behaviour may be distinguished. Note that in each of these plots one branch of λ is exactly unity at $\xi = 0$, because of neutral stability within the family of uniform flows.

In Figure 5, the solution curves lie below one, i.e. $|\lambda| \leq 1$ for all ξ, so that this is a stable situation. However, in Figure 6, one solution branch lies wholly above unity: this is an unstable situation. These (partial analytical) arguments are in accord with the numerical simulations of Gipps: in the first case he showed that perturbations are damped, whereas in the latter case they are propagated. These results also indicate that flow is destabilised by reducing the estimated braking rate $\hat{B}$.

This motivates our next experiment, where we keep the parameters the same as for Figures 5 and 6, but vary $\hat{B}$, so as to find the point at which this uniform flow becomes unstable. The results are summarised in Figures 7 (for $\hat{B} = 2.86\text{ms}^{-2}$) and 8 (for $\hat{B} = 2.85\text{ms}^{-2}$): each shows $\max(|\lambda_-|, |\lambda_+|)(\xi)$.

These experiments indicate an instantaneous loss of stability for every nonzero value of ξ (i.e. a loss of instability to every finite wavelength disturbance). Further, they show that for these parameter values, $\xi = \pi$ is the most unstable mode, because $\max(|\lambda_-|, |\lambda_+|)(\xi)$ attains its maximum at $\xi = \pi$ in the unstable plot. More importantly: if the flow is unstable, i.e. if $\max(|\lambda_-|, |\lambda_+|)(\xi) > 1$ for some ξ, then it appears that $\max(|\lambda_-|, |\lambda_+|)(\pi) > 1$. We have performed many other numerical calculations which are in accord with this result: however, we have no proof. This result indicates that the stability/instability of the $\xi = \pi$ mode determines the stability of the flow as a whole. Hence we analyse this situation in more detail in Section 5.3.

We close here with Figures 9 and 10. These figures give the stability diagrams for parameters $B = 3.4\text{ms}^{-2}$, $\tau = 2/3\text{s}$, $\theta = 1/3\text{s}$, $\hat{B} = 3.1\text{ms}^{-2}$ (which are the mean values suggested by Gipps as suitable for real highway simulation) and flow speeds $v^* = 20\text{ms}^{-1}$ and $v^* = 5\text{ms}^{-1}$ respectively. In the first case we see that the flow is unstable, but the latter (much slower) flow is stable. Thus $\hat{B}$ is not the only parameter affecting stability: in the next section we provide a complete analysis of the roles of all the parameters.

5.3 Short wavelength perturbations: $\xi = \pi$

In Section 5.2 we showed numerically that the stability of the $\xi = \pi$ mode, which corresponds to short wavelength perturbations which repeat every second vehicle, governs the stability of uniform flow. Hence we now perform an explicit analysis of this mode.

We proceed by substituting $\xi = \pi$ (so that $w = -1$) in the characteristic equation (4.10), to yield

$$\lambda^2 - \{1 - \tau(\partial_1 F) + (\partial_2 F) - (\partial_3 F)\}\,\lambda + \{\tau(\partial_1 F) + (\partial_2 F) - (\partial_3 F)\} = 0, \tag{5.6}$$

and solution by the usual explicit formula gives

$$\lambda = \frac{1}{2}\{1 - \tau(\partial_1 F) + (\partial_2 F) - (\partial_3 F)\} \pm \frac{1}{2}\sqrt{\Big[\{1 + \tau(\partial_1 F) - (\partial_2 F) + (\partial_3 F)\}^2 - 8\tau(\partial_1 F)\Big]}, \tag{5.7}$$

on some rearrangement of the discriminant. It may be shown that for the standard Gipps model,

$$v^* > \frac{5\hat{B}\tau}{2}, \tag{5.8}$$

is sufficient for a positive discriminant, giving rise to real λ. The proof of this fact is relegated to Appendix A. However, we note here that for the parameter values suggested in [6], (5.8) implies a critical speed of 5ms^{-1}, and in practice we are always interested in faster flows than this. Hence from now on, we assume that the discriminant is positive. Thus we obtain two solutions

$$\lambda_- := -\{\tau(\partial_1 F) - (\partial_2 F) + (\partial_3 F)\} + \frac{\epsilon}{2}, \qquad < \qquad \lambda_+ := 1 - \frac{\epsilon}{2}, \tag{5.9}$$

where

$$0 < \epsilon < 1 + \tau(\partial_1 F) - (\partial_2 F) + (\partial_3 F). \tag{5.10}$$

It follows that neither root can pass through $+1$, and the onset of instability is defined by $\lambda_- = -1$. Substitution of $\lambda = -1$ in (5.6) gives

$$(\partial_3 F) - (\partial_2 F) = 1, \tag{5.11}$$

which using (4.4) for the standard Gipps model yields

$$\left(\frac{1}{\hat{B}} - \frac{1}{B}\right) v^* = \theta. \tag{5.12}$$

This equation identifies a relation between parameters which must hold at the onset of instability. Since the numerics of Section 5.2 indicated that decreasing $\hat{B}$ destabilises flow, then we obtain conditions

$$\theta < \left(\frac{1}{\hat{B}} - \frac{1}{B}\right) v^*, \qquad \text{for instability, supplemented by}$$
$$\left(\frac{1}{\hat{B}} - \frac{1}{B}\right) V^{\max} < \tau + \theta, \qquad \text{for a well defined speed-headway function (see (3.13)).} \tag{5.13}$$

Since $v^* < V^{\max}$, we identify an interesting range of useful parameter values, where a uniform flow is unstable (as there is at least one unstable mode), yet the speed-headway function is properly defined at all headway arguments. From (5.13) we may see that uniform flow is destabilised by

- decreasing the estimated maximum braking rate $\hat{B}$,
- increasing the actual maximum braking rate B,
- increasing the speed of the flow v^*,

- or decreasing the safety margin θ.

Note that for flow to be unstable, we require $B > \hat{B}$, corresponding to drivers underestimating the rate of braking of the vehicle ahead. Further, decreasing $\hat{B}$ or $\tau + \theta$ too far, or increasing B too much, leads to uniform flow which is not well defined. However, the interval of unstable but well defined uniform flow may be expanded by decreasing the safety margin θ, whilst holding $\tau + \theta$ (and hence the speed-headway function) constant. However, in the next section we present simulations which indicate problems with global dynamics when θ is decreased.

6 Numerical simulations

Here we are concerned with the numerical simulation of the full system of maps (2.11) for the standard Gipps model (2.1). Our toy system consists of $N = 50$ vehicles placed on a circular road, so that the vehicle with index 1 follows the vehicle with index 50.

For each simulation, we prescribe initial data for displacements and velocities which correspond to a uniform flow solution with speed $v^* = 20\text{ms}^{-1}$, with uniformly distributed random perturbations added to vehicles' velocities. For each vehicle, we take maximum speed $V^{\max} = 30\text{ms}^{-1}$ (a little over the UK speed limit of 70 miles per hour), the length of vehicles $S = 6.5\text{m}$, and the acceleration parameter $A = 1.7\text{ms}^{-2}$.

We present the results of six simulations in total. The first four simulations have all vehicles identical. Experiment 1 illustrates a stable uniform flow. In contrast, Experiment 2 illustrates an unstable uniform flow scenario, where the model produces *travelling waves*.

Experiments 3 and 4 depict parameter regimes in which Gipps' model may lose global existence in time. This occurs by the solutions evolving so that at some time, the action of taking a square root in (2.1) gives rise to an imaginary candidate velocity: beyond such a time solutions are unphysical.

In Experiments 5 and 6, we allow vehicles to differ by assigning to them a uniformly distributed random variable for the estimated braking rate $\hat{B}$. Depending on the mean value of $\hat{B}$, we observe either travelling wave solutions, or uniform flow. These two types of stable $t \to \infty$ solutions seem remarkably robust considering vehicles' characteristics are allowed to differ. This justifies our analysis of the simplified situation where all vehicle characteristics are equal.

Experiment 1: stable uniform flow. We take $B = 3.0\text{ms}^{-2}$, $\tau = 2/3\text{s}$, $\theta = 1/3\text{s}$, and $\hat{B} = 3.5\text{ms}^{-2}$, which were the parameters chosen for the first eigenvalue computation of Section 5.2. We apply large $\pm 70\%$ noise to the initial uniform flow velocity. Figure 11 plots the displacements of vehicles (modulo the length of the circular road) against time. We see that the initial variations in velocity die out rapidly, and the solution converges to a uniform flow, where trajectories in the (t, x) plane are parallel. This is what we expect: equation (5.13) indicates that this uniform flow is stable (and also that the speed-headway function is well defined).

Experiment 2: unstable uniform flow, leading to a travelling wave. We take the same parameters as Experiment 1, but reduce the estimated braking rate to $\hat{B} = 2.8\text{ms}^{-2}$. Criteria (5.13) indicate that for $2.85714\ldots > \hat{B} > 2.72727\ldots$, this uniform flow is unstable and the speed-headway function is well-defined. Figure 12(a) shows the (t, x) plot: indeed the uniform flow solution is unstable and we observe the formation of a *travelling wave*, which propagates around the circular road in an upstream direction. (Note that the speed of this wave is more than 10ms^{-1}, which faster than those observed in real traffic: see e.g. Abou-Rahme (1999) [1, Sec. 2.2] who found a typical wave speed to be 19 kilometres per hour. However, we anticipate that a more careful choice of parameters will produce a better value.) Figure 12(b) shows the velocity against time of vehicle 1 as it performs a number of laps and passes in and out of the wave structure. The velocity varies periodically between about 12ms^{-1} and 29ms^{-1}, with a gradual acceleration and abrupt braking linking these extremes. This behaviour resembles the stop-start nature of real highway traffic: however the deceleration produced here is unrealistically high.

Figure 13 gives more detail of the structure of the travelling wave solution. Figure 13(a) is a discrete time plot of the velocity v of vehicle 1 against its headway h, upon which a graph of the effective speed-headway function $V(h)$ has been superimposed. One observes that usually $v < V(h)$, and the vehicle is accelerating. However, owing to a hard braking of the vehicle in front, the headway is suddenly decreased and then $v > V(h)$. Hard braking then follows. The acceleration procedure then repeats.

Figure 13(b) is similar, except that the velocity v_2 of vehicle 2 is plotted against the velocity v_1 of vehicle 1 (which is immediately ahead). The line $v_2 = v_1$ is added to the figure. For much of the time vehicle 2 is travelling slower than vehicle 1 and is accelerating: however, vehicle 1 then brakes sharply, leaving vehicle 2 travelling faster, and thus breaking sharply at the next time step.

From Figure 13 it may be seen that the travelling wave solution visits both regimes of (2.1). During most of the loop, we have the car-following regime where velocity is limited by the vehicle ahead. However, following the sharp braking, the free acceleration regime is possible for a short time.

We should add one further remark: from (5.13), we see that the linear stability of uniform flow is unaffected by the parameters $V^{\max}$, A, and S. However, we have observed in other experiments that these parameters do have an impact on the global solution patterns which result when uniform flow is unstable. For example, increasing $V^{\max}$ will lead to higher speeds being attained, or alternatively reducing the acceleration parameter A will lead to smoother, smaller amplitude waves.

Experiment 3: loss of global existence as $\hat{B}$ is decreased. We take the same parameters as for Experiments 1 and 2, but reduce $\hat{B}$ to 2.72ms^{-2}; i.e. below the limit for the speed-headway function to be well defined, in the sense defined in Section 3. We now incorporate just 5% noise in the uniform flow initial condition. Figure 14(a) gives the (t, x) plot. As for Experiment 2, we see the instability of uniform flow, and the rapid formation of travelling waves. All appears well. However Figure 14(b), which plots the contents of the square root arising in the second regime of (2.1), minimised over all vehicles, indicates a problem. This quantity hits zero (and then becomes negative) in finite time. This results in a complex candidate velocity in (2.1), and at that instant Gipps' model becomes unphysical.

We have performed a number of simulations of this kind, and our working conjecture is that such a loss of global existence will not occur, provided the second condition of (5.13) is satisfied (so that the speed-headway function is well defined), and provided the noise added to the uniform flow initial data is sufficiently small.

Thus it seems that there is only a small interval of $\hat{B}$ where uniform flow is unstable, yet where there is also global existence in time. Examining (5.13), it seems that this interval of 'interesting' $\hat{B}$ can be increased, if the safety margin θ is decreased. Recall (from Section 3) that if this is achieved by holding $\tau + \theta$ constant, then the speed-headway function (which presumably one would fit to real world data) is unchanged. This motivates our next experiment.

Experiment 4: loss of global existence as θ is decreased. We take most parameters as for preceding experiments, but set $\tau = 5/6\text{s}$, $\theta = 1/6\text{s}$, and set $\hat{B} = 2.8\text{ms}^{-2}$. We add 5% noise to the uniform flow initial data. According to (5.13), this is an unstable situation where the speed-headway function is well-defined. Figure 15 depicts the results. One observes that a travelling wave begins to develop, but then, as for Experiment 3, the model loses feasibility. Therefore, our conjecture, which links the well-definedness of the speed-headway function and the global existence of a solution, does not apply if θ is reduced. Indeed, Gipps himself realised that $\theta = \tau/2$ was a special case (he found no crashes for this choice).

In our last two simulations, we no longer require that all vehicles/drivers are identical. There are many ways in which one could break this symmetry: as a simple illustration, we allow only the estimated braking rate $\hat{B}$ to vary from vehicle to vehicle, and we require that the other parameters are the same for all cars and equal to the choices set in Experiment 1.

Experiment 5: noisy simulation, unstable flow. We assigned $\hat{B}$ according to a uniform distribution between 2.55ms^{-2} and 3.05ms^{-2}. The initial condition was a uniform flow derived by (falsely) assuming that all vehicles had $\hat{B} = 2.8\text{ms}^{-2}$ (the mean value), with 5% noise added to velocities. Figure 16 gives the (t, x) plot, and the velocity of vehicle 1 against uniform time. We see that uniform flow is unstable (indeed the initial data is not actually a solution, because of the variation in $\hat{B}$ between drivers), which is not too surprising given that the mean of $\hat{B}$ lies in the unstable regime according to (5.13). However, given the variations between vehicles (some as individuals are stable, others are strongly unstable), it is surprising that such a regular travelling wave structure arises.

Experiment 6: noisy simulation, stable flow. We assigned $\hat{B}$ according to a uniform distribution between 2.65ms^{-2} and 3.15ms^{-2}, and provided initial data in the same manner as for Experiment 5. The mean of $\hat{B}$ is now 2.9ms^{-2}, which according to (5.13) is a stable value. Figure 17 shows the resulting stable uniform flow solution. Note that the curves in this (t, x) diagram are (eventually) parallel, indicating that all vehicles travel at the same speed. However, because $\hat{B}$ (and hence the speed-headway function) varies from vehicle to vehicle, the headways of vehicles are not equal. As in Experiment 5, it is surprising that

there is such regular solution behaviour, given the variation between drivers.

7 Conclusions and further work

Here we have derived the speed-headway function for Gipps model, and presented a linear stability analysis of the uniform flow solutions. We have also shown simulation results indicating interesting solution behaviour when uniform flow is unstable.

More work is required to develop an understanding of the travelling wave structures. Further, is it possible to derive analytical conditions which guarantee the global $t > 0$ existence of physical solutions?

It might also be interesting to derive and simulate other *Gipps-like* models of the form of (2.2), where the appropriate monotonicity conditions are satisfied.

Acknowledgement

Many thanks to my Master of Science student Steve Hooper, for correcting the speed-headway function calculation in Section 3. Thanks also to Jo White of the Transport Research Laboratory for interesting discussion.

References

[1] N.F. Abou-Rahme, A probabilistic model for the origin of motorway shockwaves, doctoral transfer thesis, University of Southampton (1999).

[2] M. Bando et al, Dynamical model of traffic congestion and numerical simulation, *Phys. Rev. E.* **51** (1995) 1035–1042.

[3] R.E. Chandler, R. Herman and E.W. Montroll, Traffic dynamics; studies in car following, *Opns. Res.* **6** (1958) 165–184.

[4] S. Druitt, An introduction to Paramics microsimulation, `http://www.sias.co.uk/sias/paramics/part1.html`, SIAS Ltd (2000).

[5] D.C. Gazis, R. Herman and R. Rothery, Non-linear follow-the-leader models of traffic flow, *Opns. Res.* **9** (1961) 545–567.

[6] P.G. Gipps, A behavioural car-following model for computer simulation, *Transpn. Res.-B* **15B** (1981) 105–111.

[7] E.N. Holland, A generalised stability criterion for motorway traffic, *Transpn. Res.-B* **32** (1998) 141–154.

[8] A.D. Mason and A. W. Woods, Car-following model of multispecies systems of road traffic, *Phys. Rev. E* **55** (1997) 2203–2214.

[9] The Highway Code, Driving Standards Agency (1999). Published by the UK government Stationery Office.

[10] SISTM: a motorway simulation model, Leaflet LF2061, Transport Research Laboratory (1993).

A Positivity of the discriminant

Here we derive a sufficient condition for the positivity of the discriminant

$$d := \{1 + \tau(\partial_1 F) - (\partial_2 F) + (\partial_3 F)\}^2 - 8\tau(\partial_1 F), \tag{A.1}$$

of formula (5.7), when the standard Gipps model is in force. (This was a necessary part of the explicit stability analysis of the $\xi = \pi$ mode in Section 5.3.)

Using (4.4), we obtain

$$d = \frac{\left[\left\{\frac{v^*}{B} + \left(\frac{\tau}{2} + \theta\right)\right\} + \left\{\frac{3\tau}{2} + \frac{v^*}{\hat{B}}\right\}\right]^2 - 8\tau\left\{\frac{v^*}{B} + \left(\frac{\tau}{2} + \theta\right)\right\}}{\left\{\frac{v^*}{B} + \left(\frac{\tau}{2} + \theta\right)\right\}^2}, \tag{A.2}$$

whose numerator D has the same sign as d and may be written

$$D = \left\{\frac{v^*}{B} + \left(\frac{\tau}{2} + \theta\right)\right\}^2 + \left\{\frac{3\tau}{2} + \frac{v^*}{\hat{B}}\right\}^2 + \left\{2\frac{v^*}{\hat{B}} - 5\tau\right\}\left\{\frac{v^*}{B} + \left(\frac{\tau}{2} + \theta\right)\right\}. \tag{A.3}$$

Only one of the braces has indeterminate sign. Thus a sufficient condition for $D > 0$ (and hence $d > 0$) is

$$v^* > \frac{5\hat{B}\tau}{2}. \tag{A.4}$$

Using typical values of $\tau = 2/3$s and $\hat{B} = 3\text{ms}^{-1}$ implies positivity of the discriminant if the uniform flow speed v^* exceeds 5ms^{-1}.

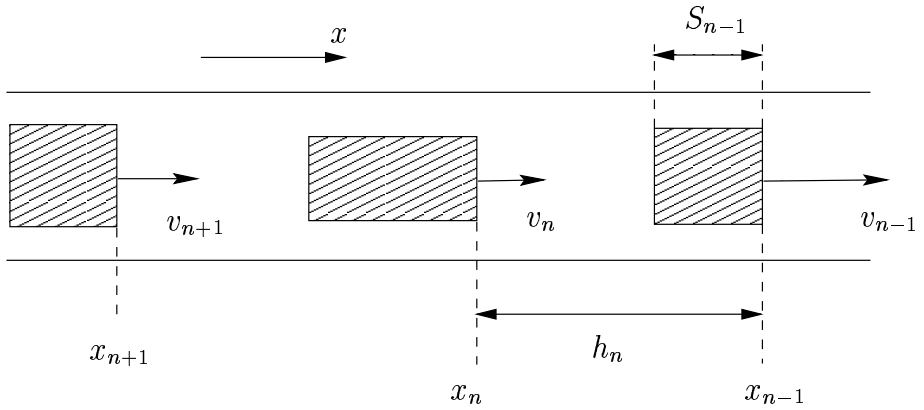

Figure 1: Definitions of displacement x, velocity v, headway h, and length of vehicle S. Vehicles travel to the right in an increasing x direction.

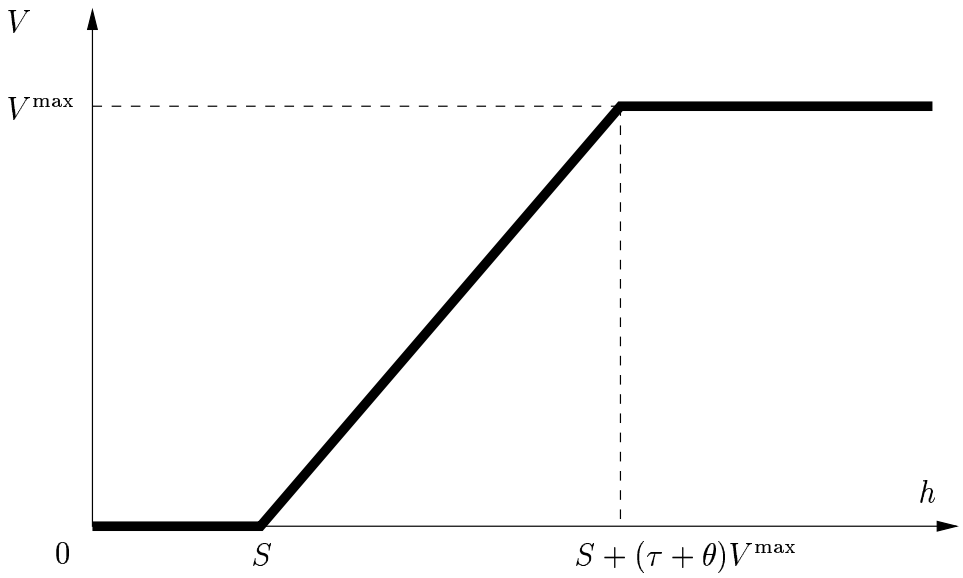

Figure 2: Sketch of speed-headway function for $B = \hat{B}$. See equation (3.9).

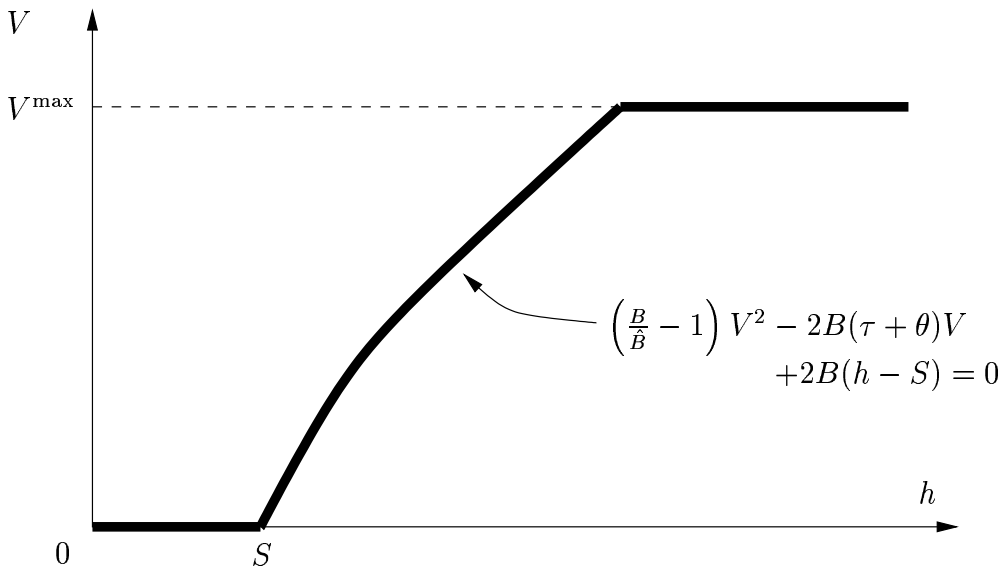

Figure 3: Sketch of speed-headway function for $B < \hat{B}$. See equation (3.12).

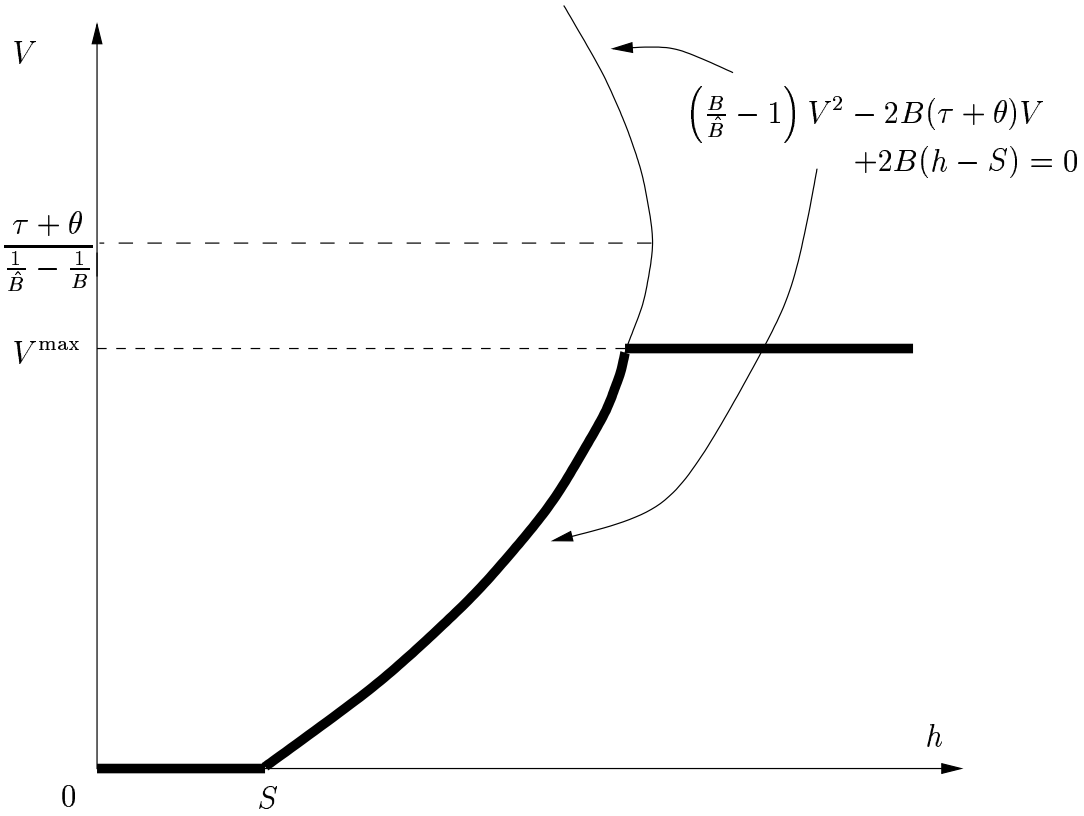

Figure 4: Sketch of speed-headway function for $B > \hat{B}$. This is not well defined if $V^{\max} > (\tau+\theta)/(1/\hat{B}-1/B)$. See equation (3.14).

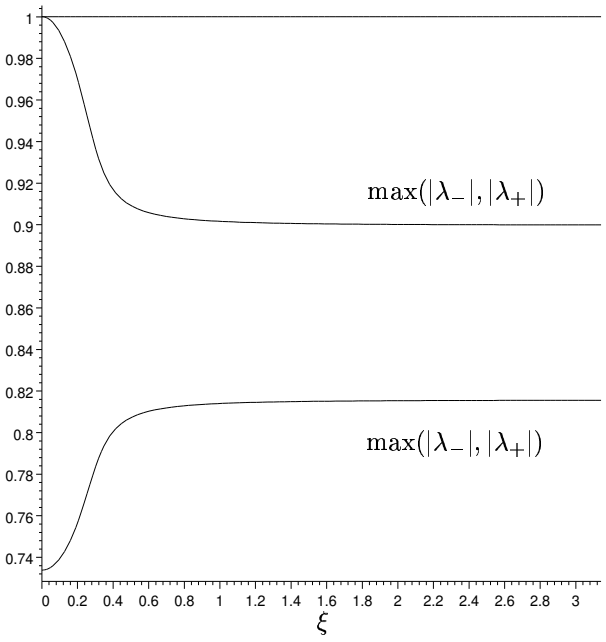

Figure 5: Eigenvalue plot for $B = 3.0\text{ms}^{-2}$, $\tau = 2/3\text{s}$, $\theta = 1/3\text{s}$, $v^* = 20.0\text{ms}^{-1}$, and $\hat{B} = 3.5\text{ms}^{-2}$. See Section 5.2. This uniform flow is stable because $|\lambda(\xi)| \leq 1$ for all ξ.

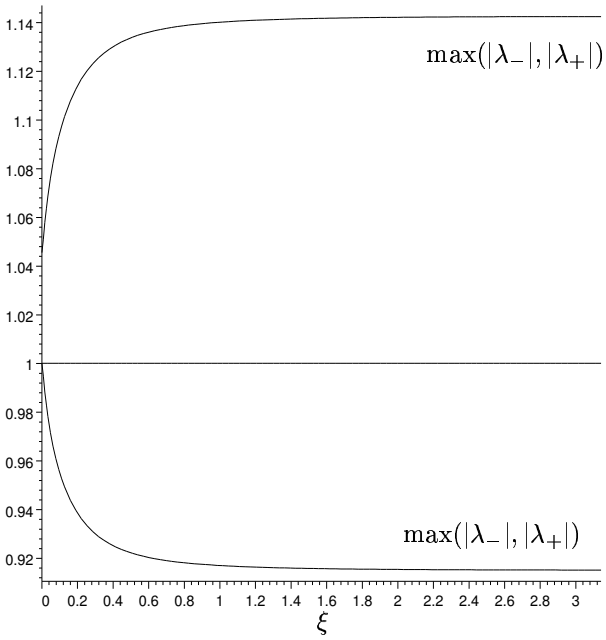

Figure 6: Eigenvalue plot: as for Figure 5 except $\hat{B} = 2.5\text{ms}^{-2}$. Flow is unstable because there are eignevalues with modulus exceeding one.

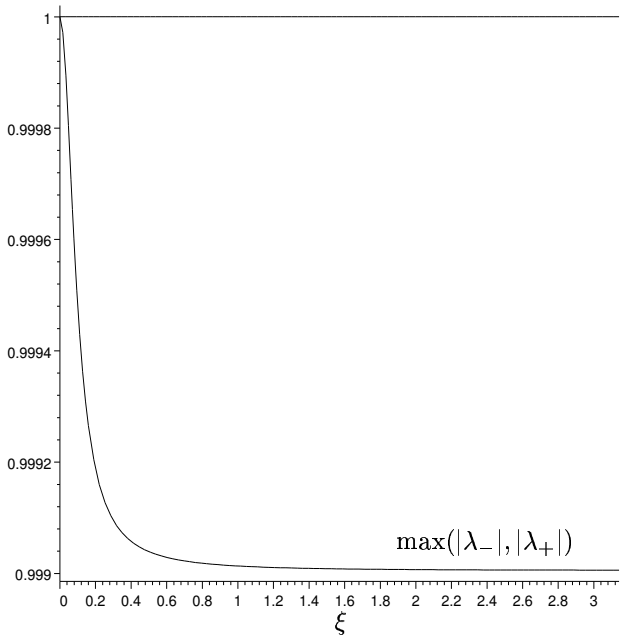

Figure 7: Eigenvalue plot: parameters as for Figure 5, but with $\hat{B} = 2.86\text{ms}^{-2}$. The uniform flow is stable.

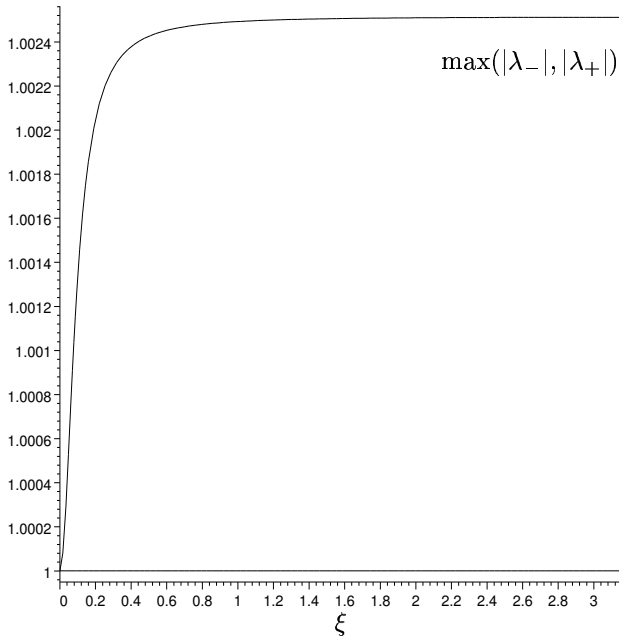

Figure 8: Eigenvalue plot: parameters as for Figure 5, but with $\hat{B} = 2.85\text{ms}^{-2}$. Compare with Figure 7. Note that $\xi = \pi$ is the most unstable mode, in the sense that if $\max(|\lambda_-(\xi)|, |\lambda_+(\xi)|) > 1$ for some ξ, then $\max(|\lambda_-(\pi)|, |\lambda_+(\pi)|) > 1$.

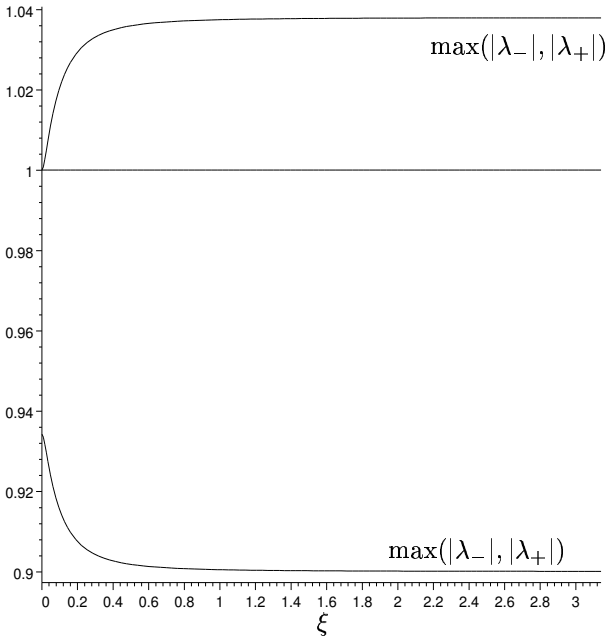

Figure 9: Eigenvalue plot: $B = 3.4\text{ms}^{-1}$, $\tau = 2/3\text{s}$, $\theta = 1/3\text{s}$, $\hat{B} = 3.1\text{ms}^{-2}$, and $v^* = 20\text{ms}^{-1}$: uniform flow is unstable.

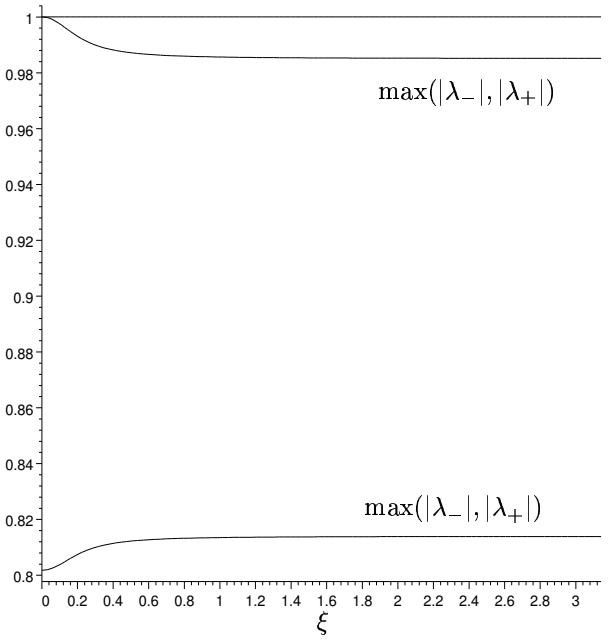

Figure 10: Eigenvalue plot: parameters as for Figure 9, except $v^* = 5\text{ms}^{-1}$. This slower uniform flow is stable.

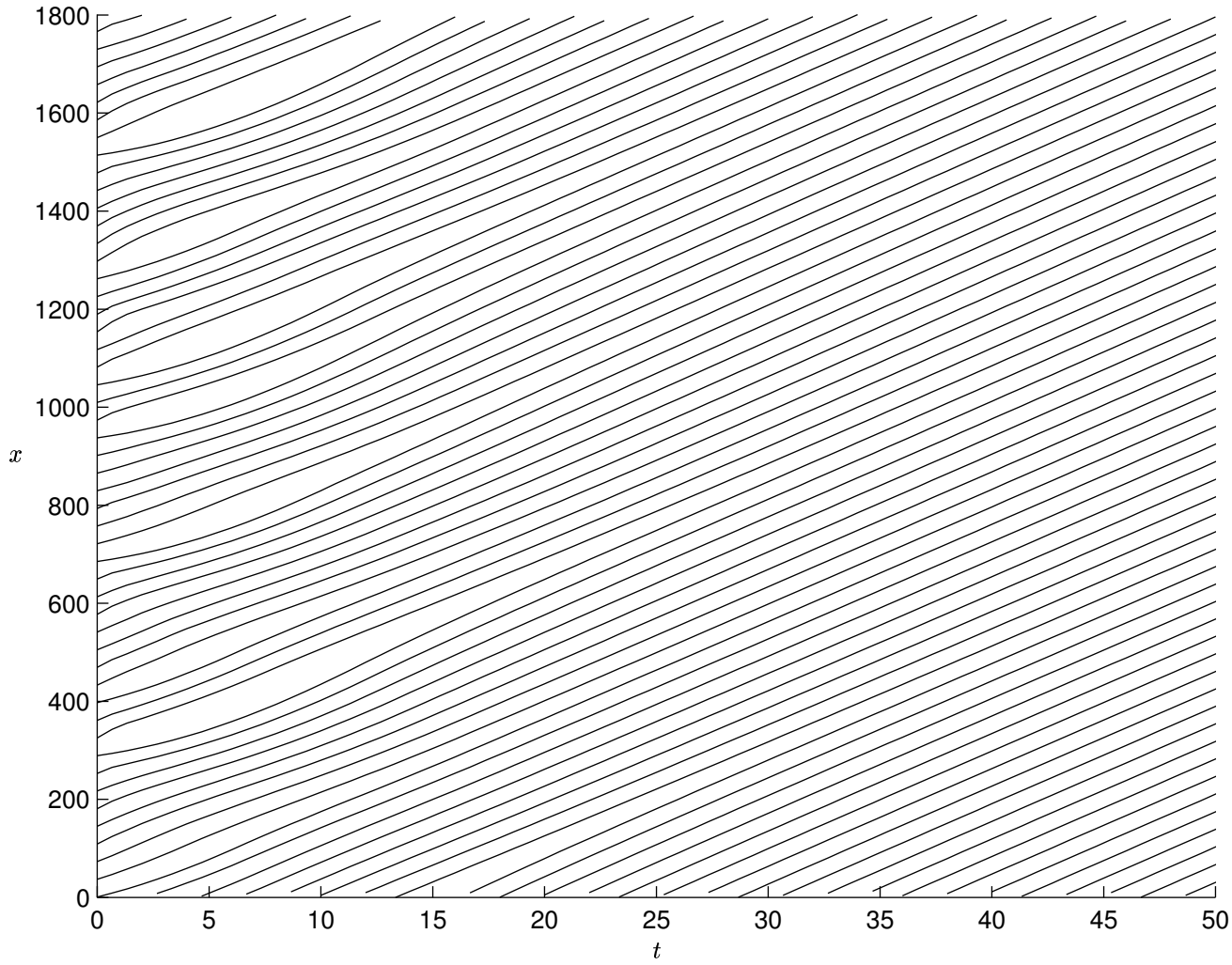

Figure 11: A simulation where uniform flow is stable. See Experiment 1. The displacement x of vehicles (modulo the length of the circular road) is plotted against time t.

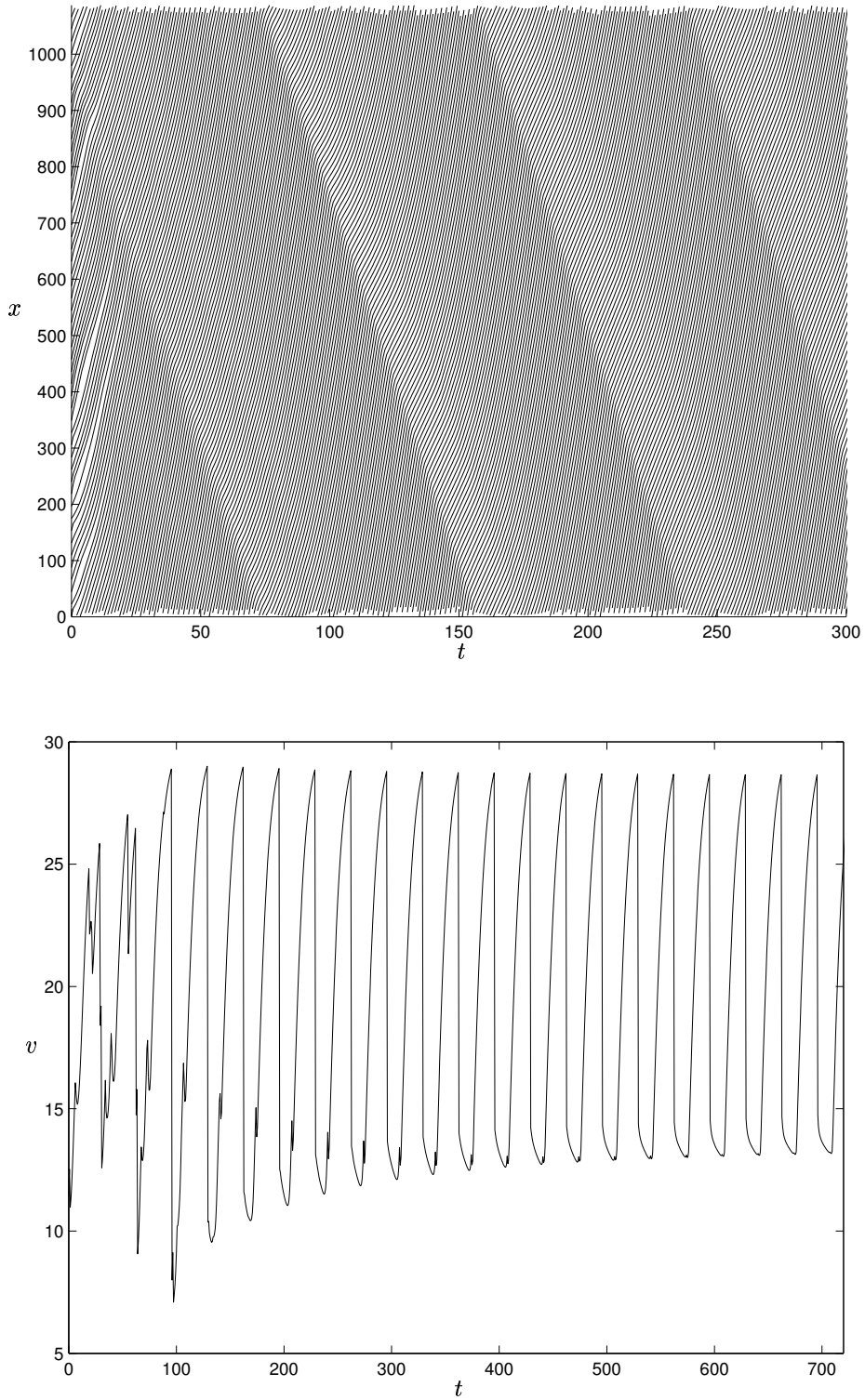

Figure 12: (a) Unstable uniform flow and the evolution of travelling waves. See Experiment 2. (b) The velocity of a vehicle as it passes repeatedly through the wave structure.

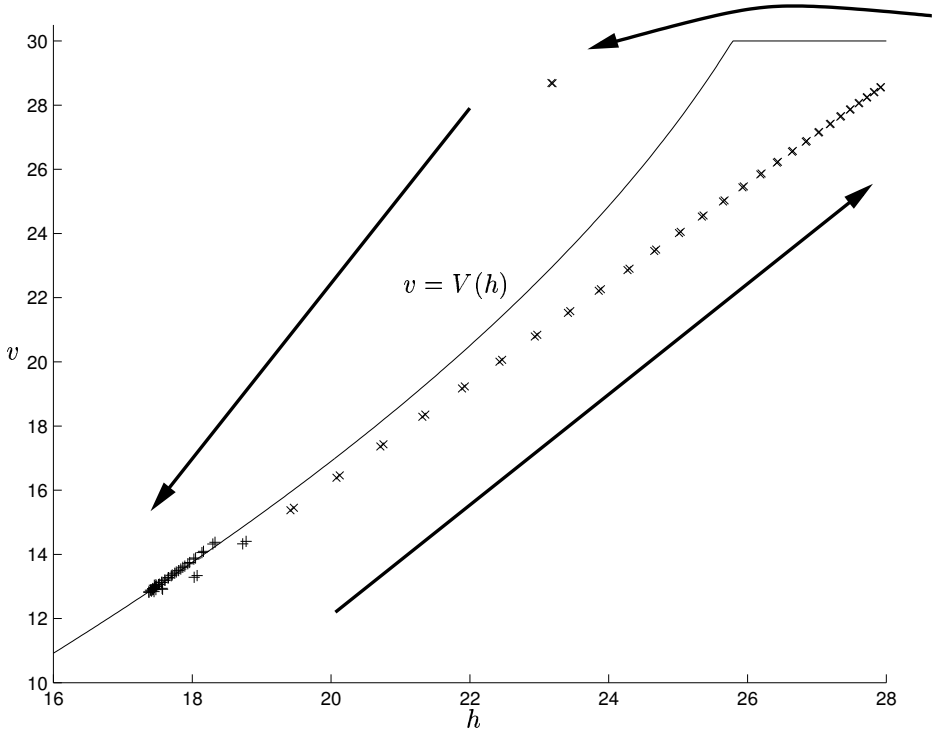

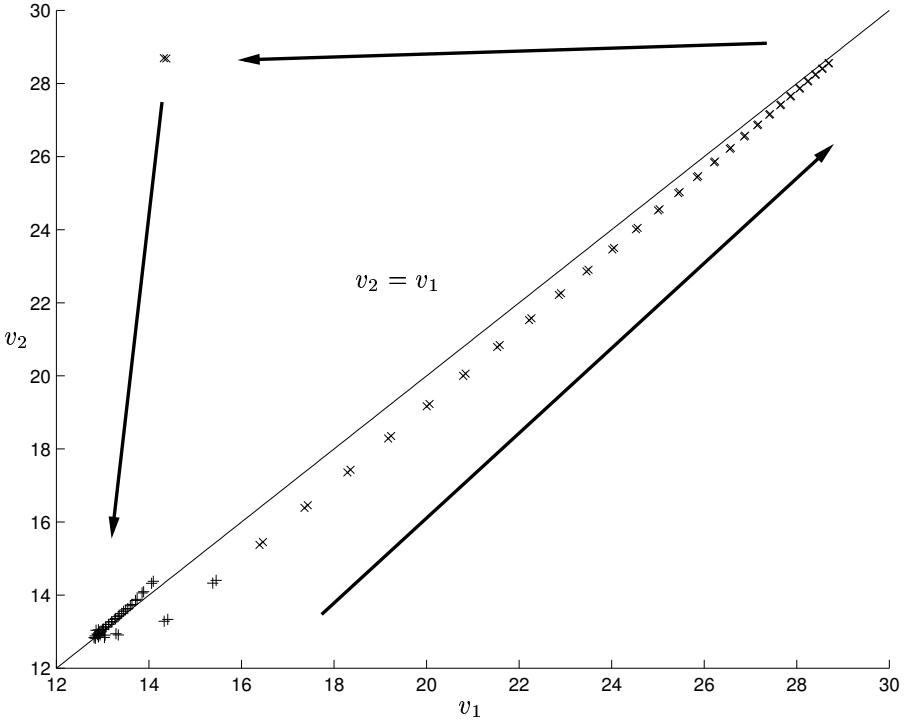

Figure 13: Experiment 2 continued. (a) Velocity against headway for an individual vehicle, with the speed-headway graph added. (b) The relation between velocities of two consecutive vehicles. In these figures, '+' denotes points the first (freely accelerating) regime of (2.1). '×' denotes the second (car-following, i.e., velocity limited by vehicle ahead) regime.

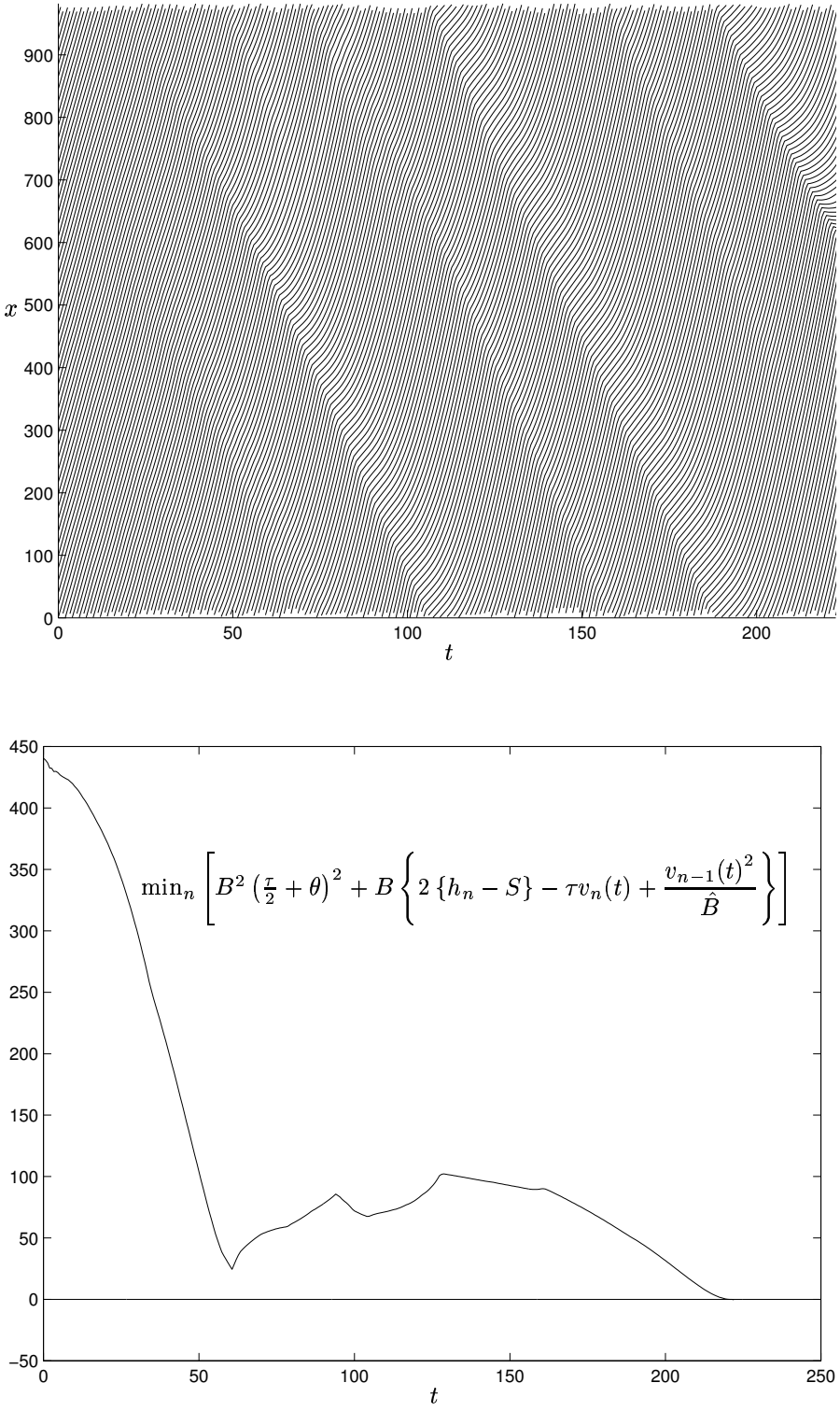

Figure 14: See Experiment 3. (a) Travelling waves start to form. (b) The solution becomes unphysical in finite time, as a complex quantity appears in equation (2.1).

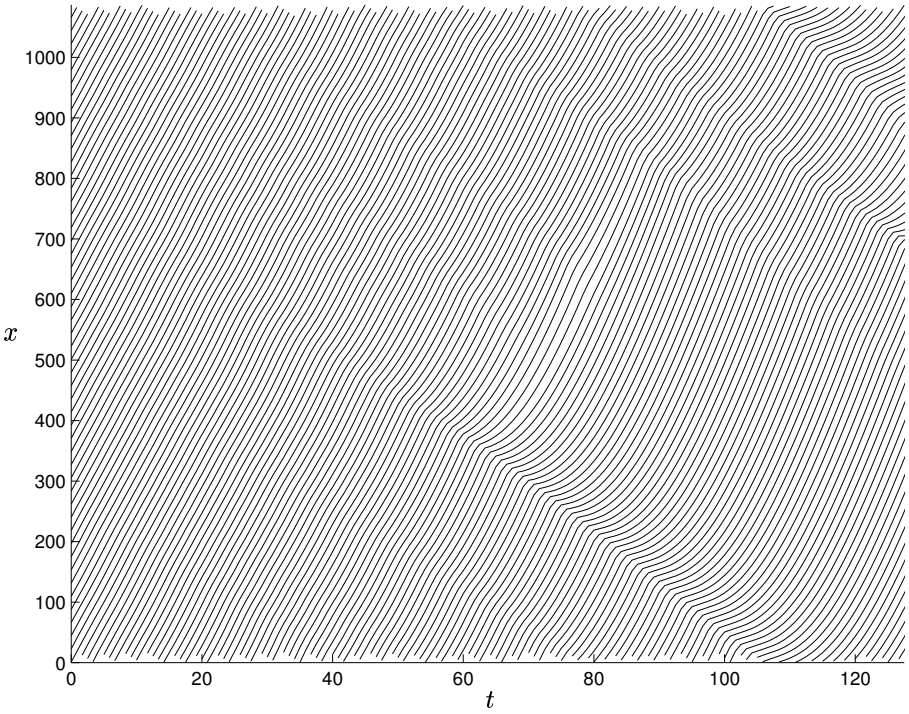

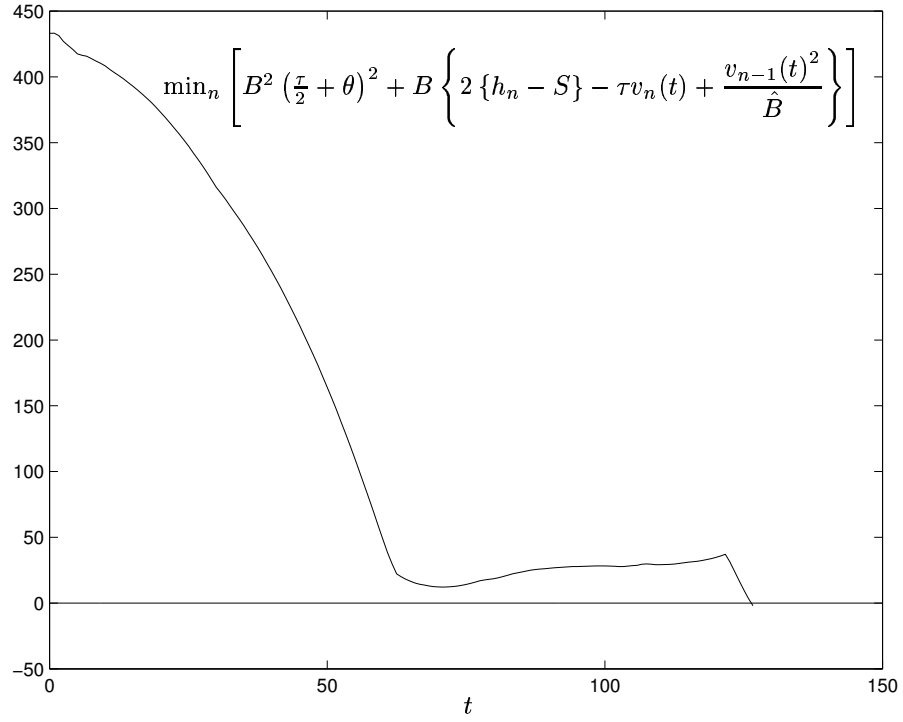

Figure 15: See Experiment 4. A similar situation to Figure 14. Again travelling waves start to form, but the solution becomes complex and hence unphysical.

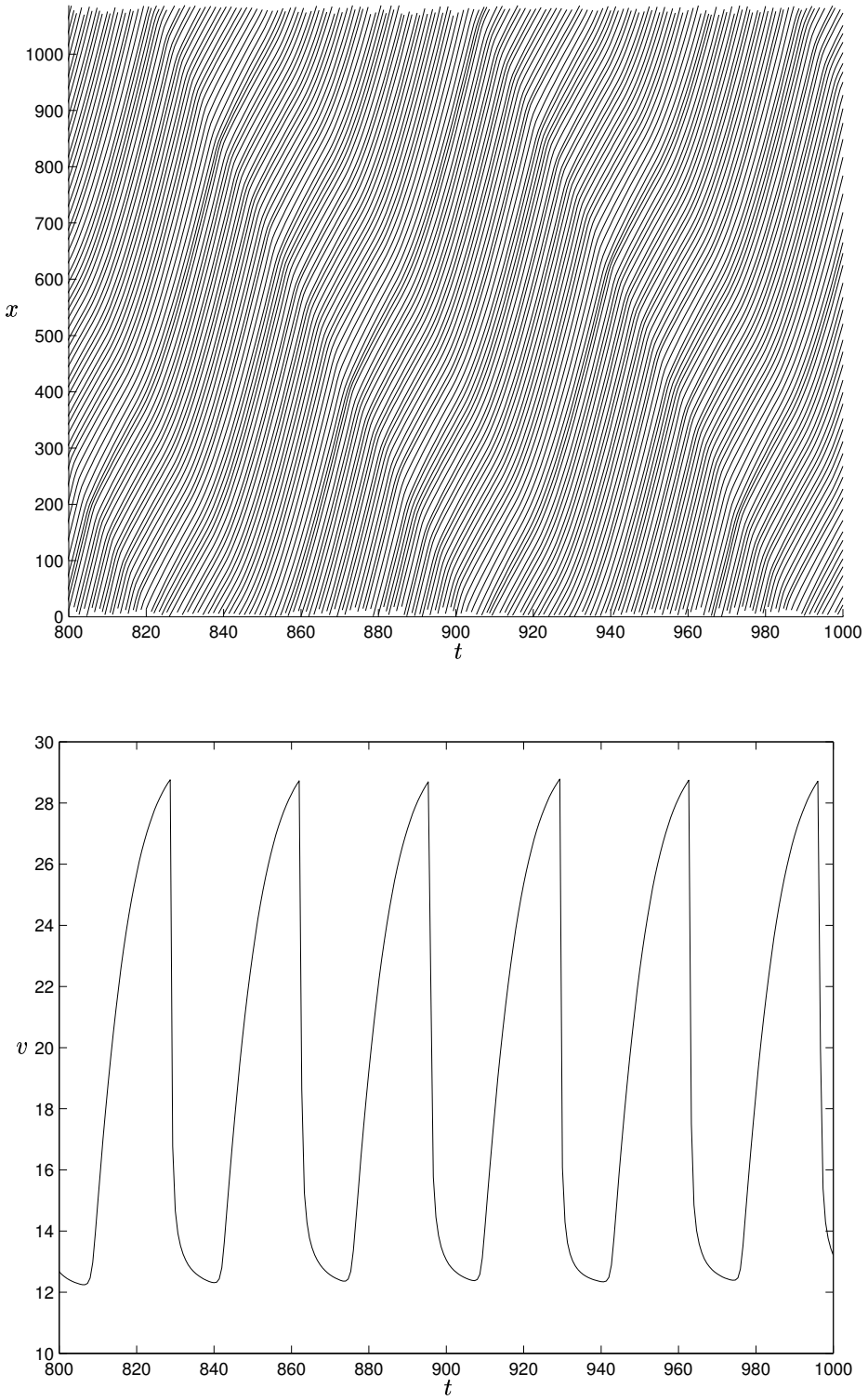

Figure 16: See Experiment 5. (a) Travelling waves when vehicle characteristics are allowed to differ. (b) The velocity against time of a single vehicle passing repeatedly through the travelling wave.

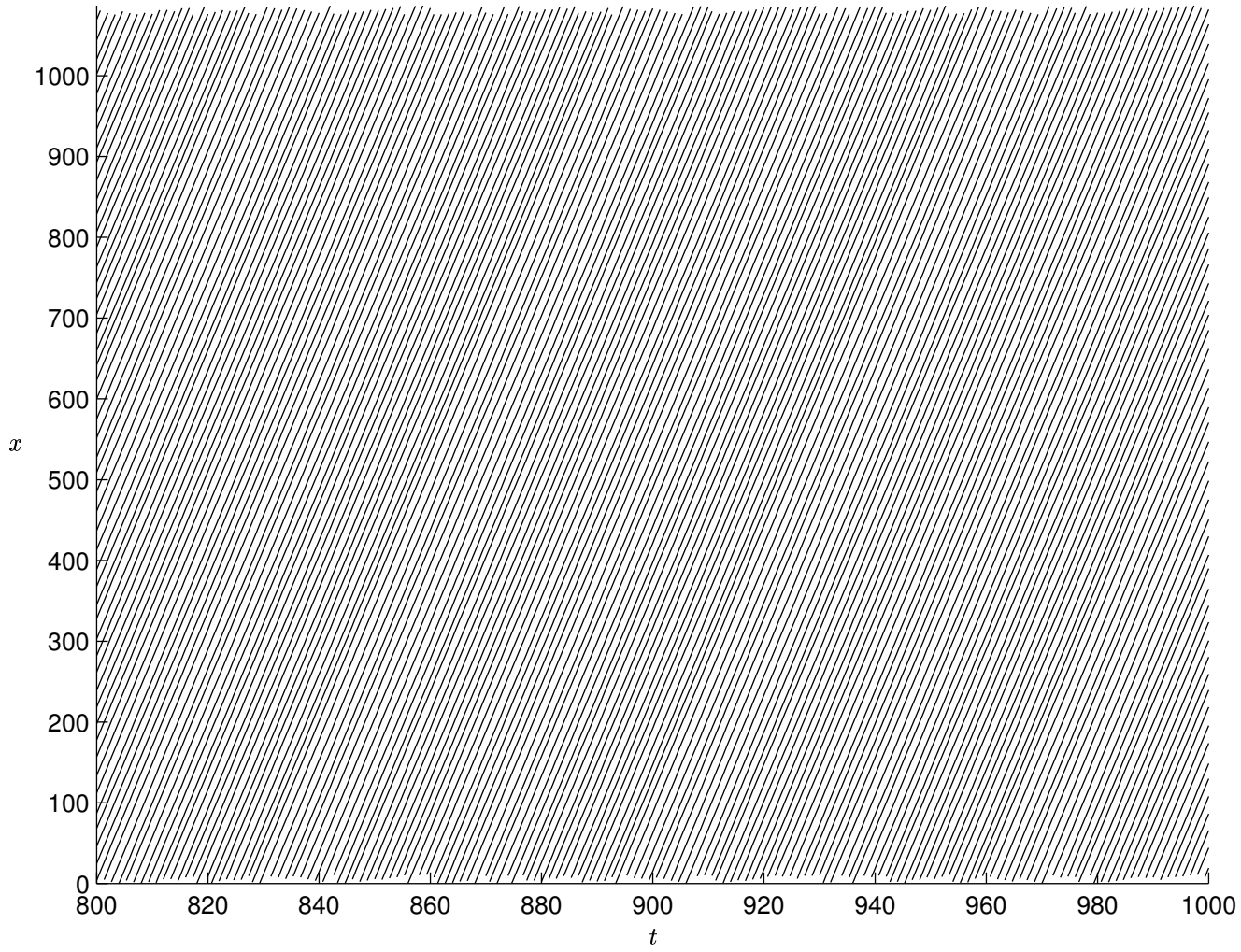

Figure 17: See Experiment 6. Vehicles differ, but a uniform flow solution evolves where all vehicles have the same speed, albeit different headways.